Raman scattering in $CaFeO_3$ and $La_{0.33}Sr_{0.67}FeO_3$ across the charge-disproportionation phase transition

Shankar Ghosh,[1] N. Kamaraju,[1] M. Seto,[2] A. Fujimori,[3] Y. Takeda,[4] S. Ishiwata,[5] S. Kawasaki,[5] M. Azuma,[5] M. Takano,[5] and A. K. Sood[1,*]

[1]Department of Physics, Indian Institute of Science, Bangalore 560 012, India
[2]Research Reactor Institute, Kyoto University, Kumatori-cho, Osaka 590-0494, Japan
[3]Department of Physics and Department of Complexity Science and Engineering, University of Tokyo, Bunkyo-ku, Tokyo 113-0033, Japan
[4]Department of Chemistry, Mie University, Tsu 514-8507, Japan
[5]Institute of Chemical Research, Kyoto University, Uji, Kyoto 611-0011, Japan

Temperature-dependent micro-Raman studies of orthorhombic $CaFeO_3$ and rhombohedral $La_{0.33}Sr_{0.67}FeO_3$ were carried out with an aim to study the role of a lattice in the formation of the charge-disproportioned state ($Fe^{4+} \rightarrow Fe^{5+} + Fe^{3+}$) below the transition temperature (T_{co}) of 290 and 200 K, respectively. Shell-model lattice-dynamical calculations were performed for $CaFeO_3$ to assign the Raman modes and determine their vibrational pattern. The temperature dependence of the peak positions and the peak widths of various modes for both systems show distinct changes across their respective transition temperatures. In $CaFeO_3$, the symmetric-stretching mode at 707 cm^{-1} splits into two modes, 707 cm^{-1} and 684 cm^{-1}, corresponding to the breathing-type distortion of the FeO_6 octahedra. In comparison, the spectral feature at 704 cm^{-1} in $La_{0.33}Sr_{0.67}FeO_3$, which has been assigned to the Raman-forbidden symmetric-stretching mode, disappears below T_{co}. These observations indicate the presence of finite Jahn-Teller distortions of the FeO_6 octahedra in $CaFeO_3$ in the entire temperature range, whereas these distortions are present only above T_{co} in $La_{0.33}Sr_{0.67}FeO_3$. Two modes at 307 cm^{-1} and 380 cm^{-1} in $La_{0.33}Sr_{0.67}FeO_3$ approach each other at T_{co}, indicating a reduction of rhombohedral distortions below T_{co}.

I. INTRODUCTION

In recent years, strongly electron correlated three-dimensional (3D) transition-metal oxides have revealed a rich variety of interesting physical phenomena, such as the metal-insulator transition and ordering of charge, spin, and orbital degrees of freedom.[1] In this class, iron pervoskites containing iron in $Fe^{4+}(d^4)$, namely $CaFeO_3$ (CFO) and $La_{0.33}Sr_{0.67}FeO_3$ (LSFO), are interesting systems in which to explore the role of electron-lattice interactions vis-à-vis the electron correlations in understanding the charge-order (CO) transition associated with charge disproportion. In these systems, the proposed electronic configuration of the FeO_6 octahedron is not $Fe^{4+}(O_6)^{12-}$, but is close to $Fe^{3+}(O_6)^{11-}$, which is expressed as $Fe^{3+}\underline{L}$ ($\underline{L}$ stands for a hole in the oxygen $2p$ orbitals). Since the ground state of Fe in these systems is predominantly $Fe^{3+}(3d^5\underline{L})$ rather than $Fe^{4+}(3d^4)$, the Jahn-Teller (JT) distortions in these systems are not expected to be large.[2] The transition of CFO from an orthorhombic metal ($T > T_{co}$) to a charge-ordered monoclinic semiconductor[3] at $T_{co} = 290$ K is associated with charge disproportion $2Fe^{3+} + \underline{L} \rightarrow Fe^{3+}$(large octahedra) $+ Fe^{3+}\underline{L}^2$(small octahedra) (nominally written as $2Fe^{4+} \rightarrow Fe^{3+} + Fe^{5+}$). As temperature is lowered further, there is another transition from the paramagnetic insulator to an antiferromagnetic insulator at $T_N = 115$ K. On the other hand, LSFO with a formal value of $Fe^{3.67}$ shows a charge-ordering transition[4] at $T_{co} = 200$ K, i.e., $2Fe^{3+}\underline{L}^{2/3} \rightarrow 2Fe^{3+} + Fe^{3+}\underline{L}^2$. The low-temperature ($T < T_{co}$) phase exhibits charge dispro-

portion with $Fe^{3+}:Fe^{5+}::2:1$ in the $\langle 111 \rangle$ direction.[5] The octahedral distortion resulting from the ordering of Fe^{3+} and Fe^{5+} states is referred to as a freezing of a breathing phonon mode. The charge-disproportioned states in both systems have been well established experimentally using Mössbauer spectroscopy.[16–18]

Recent photoemission and unrestricted Hartree-Fock band-structure calculations[4] have suggested different routes to charge disproportion in CFO and LSFO. It has been argued that both breathing and tilting distortions of FeO_6 are necessary to induce charge disproportion in CFO, whereas only electron correlations hold the key to charge disproportion in LSFO. Neutron-diffraction experiments[6] in LSFO showed that Fe-O bond lengths remain almost the same in the temperature range 300–50 K, whereas the Fe-O-Fe bond angle decreases slightly from 174° to 171°. However, more recent neutron-scattering experiments[7] show that the Fe-O bond length decreases slightly from 1.939 Å at 300 K to 1.936 Å at 15 K, while the Fe-O-Fe bond angle decreases from 173.29° to 172.89°.

Recent nuclear resonant scattering measurements[8] of CFO and LSFO showed that the phonon density of states (DOS) for both systems changes in the spectral region of 300–500 cm^{-1} across their respective T_{co}'s. However, the changes in the DOS were found to be more pronounced for CFO as compared to LSFO. The objective of the present work is to address the role of a lattice in the CO transition in these systems using Raman spectroscopy, which has been used very effectively in recent studies of magnetite[9] and

manganites[10–14] across the metal-insulator and charge-ordering transitions.

II. EXPERIENTIAL DETAILS

Polycrystalline samples of CFO and LSFO were prepared by solid-state reactions and a subsequent treatment under high-pressure oxygen, as described earlier.[15] The phase transitions as described above were characterized by electrical measurements and Mössbauer spectroscopy.[16] Confocal micro-Raman studies on these polycrystalline CFO and LSFO samples were carried out in backscattering geometry using a DILOR-XY instrument equipped with a liquid-nitrogen-cooled CCD detector. Raman spectra were recorded using 514.5 nm radiation of an argon-ion laser with a power of 5 mW using a $50\times$ long working distance objective. A temperature range of 330–4.2 K was covered using a continuous-flow helium cryostat from M/s Oxford, UK. The polycrystalline samples used consisted of irregularly shaped optically isotropic grains. It was, therefore, possible to obtain only two types of polarization spectra: HH ($E_i\|E_s$) and HV ($E_i\perp E_s$) polarizations of the incident (i) and scattered (s) electric fields (E).

III. RESULTS AND DISCUSSIONS

A. Raman spectra at room temperature

CFO is an orthorhombic crystal having a $GdFeO_3$ structure at room temperature belonging to the space group *Pnma*. It has four formula units per unit cell. The Ca ions occupy the $4c(x,1/4,z)$ site, the planar oxygen (O1) (x,y,z) ions occupy the $8d$ site, the apical oxygen (O2) ions occupy the $4c(x,1/4,z)$ site, while the Fe ions occupy the $4b(0,0,1/2)$ site. Accordingly, it has 24 zone-center Raman-active modes given by irreducible representations as $7A_g +7B_{1g}+5B_{2g}+5B_{3g}$.[12] In all these modes, Fe ions do not move. Sixteen of the 24 Raman-active modes involve vibrations of the FeO_6 octahedra, while the remaining eight modes involve motion of Ca ions.[19] In comparison, LSFO has a rhombohedral structure and belongs to the space group $R\bar{3}c$ with two formula units per unit cell. The La/Sr ions occupy the $2a(1/4,1/4,1/4)$, the O ions $6e(x,-x+1/2,1/4)$, and the Fe ions $2b(0,0,0)$ sites. The 27 optical modes are classified as $A_{1g}(R)+4E_g(R)+3A_{2u}(IR)+5E_u(IR)+2A_{1u}+3A_{2g}$.[12] Of the five Raman-active modes, four $(3E_g+1A_g)$ involve vibrations associated with the FeO_6 octahedra while the remaining E_g mode involves vibration of La/Sr ions.[11,20]

Figure 1 shows Raman spectra of CFO [panel (a)] and LSFO [panel (b)] at room temperature. It can be seen that the observed Raman spectra (shown by filled circles) can be fitted to a sum of *n*-Lorentzians (shown by solid lines, $n=8$ for CFO and $n=7$ for LSFO). The individual components are shown by dotted lines. The eight modes of CFO, labeled as $\mathbf{W}_1\cdots\mathbf{W}_8$, are 149 cm^{-1}($\mathbf{W}_1$), 197 cm^{-1}($\mathbf{W}_2$), 218 cm^{-1}($\mathbf{W}_3$), 305 cm^{-1}($\mathbf{W}_4$), 707 cm^{-1}($\mathbf{W}_5$), 844 cm^{-1}($\mathbf{W}_6$), 898 cm^{-1}($\mathbf{W}_7$), and 922 cm^{-1}($\mathbf{W}_8$). The Raman spectrum of LSFO shows seven bands labeled as $\mathbf{M}_1\cdots\mathbf{M}_7$: 251 cm^{-1}($\mathbf{M}_1$),
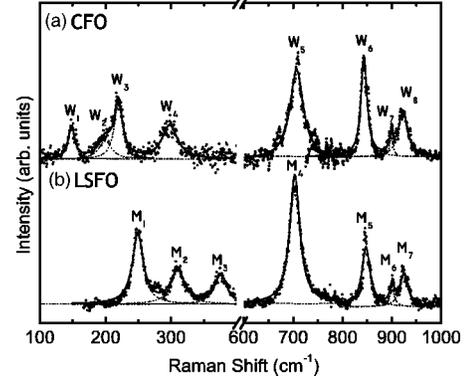

FIG. 1. Room temperature, i.e., 300 K Raman spectra of (a) CFO and (b) LSFO. The dotted lines are Lorentzian fits to the data. The CFO spectrum can be resolved into eight modes while the LSFO spectrum can be resolved into seven modes. The corresponding modes are labeled in the figure.

307 cm^{-1}($\mathbf{M}_2$), 380 cm^{-1}($\mathbf{M}_3$), 704 cm^{-1}($\mathbf{M}_4$), 843 cm^{-1}($\mathbf{M}_5$), 897 cm^{-1}($\mathbf{M}_6$), and 920 cm^{-1}($\mathbf{M}_7$). We note that both CFO (orthorhombic) and LSFO (rhombohedral) have very similar Raman spectra. Such a similarity has also been seen in the case of orthorhombic and rhombohedral manganites when Jahn-Teller distortions[11] are small. This is because the bending and tilt modes of the MnO_6 octahedra are very similar in both structures [see Figs. 4(a) and 6(b) of Ref. 11]. Before we show the temperature dependence of the modes, we will present the lattice-dynamical calculations to assign the observed Raman bands.

B. Lattice-dynamical calculations and mode assignments

The lattice-dynamics calculations (LDC) for the phonons of CFO at the Brillouin-zone center were carried out using the shell model.[21] The long-range interactions between each pair of ions were taken to be of Coulombic form, while the short-range interactions between the shells were taken to be of Born-Mayer-Buckinghan form,

$$V_{kk'}(r_{ij}) = A_{kk'}\exp(-r_{ij}/R_{kk'}) - C_{kk'}/r_{ij}^6,$$

where r_{ij} is the distance between the two ions i and j of species k and k', respectively. The parameters $A_{kk'}$, $R_{kk'}$, and $C_{kk'}$ are given in Table I. In the shell model, each ion of charge $Z|e|$ is represented by a massless shell of charge $Y|e|$ and a core of charge $(Z-Y)|e|$. The shells are elastically bound to the cores with a force constant K whose values are given in Table I. The parameters used for CFO are the same as for $CaMnO_3$,[19] except for the value of the shell charge ($Y|e|$) for Fe and O: $Y(Fe)=2.5$ as compared to $Y(Mn)=2.3$; $Y(O)=-2.1$ in CFO; and $Y(O)=-3.0$ in $CaMnO_3$. These changes in the value of Y were guided to reproduce the experimentally observed symmetric stretch vibration frequency ($\mathbf{W}_5$ mode). The reduced value of $Y(O)$ in CFO is likely due to the localization of the hole on the oxygen in these systems. Assignment of the symmetry for a normal mode vibration was determined by noting that each normal mode transforms as required by the characters of the representation to which it belongs. The character (χ) of an eigenvector, $\mathbf{E_V}$, of

ion	$Z|e|$	$Y|e|$	K (N m^{-1})	ionic pair	$A_{kk'}$ (eV)	$R_{kk'}$ (Å)	$C_{kk'}$ (eV Å^6)
Ca	1.91	3.5	1882	Ca-O	840	0.367	0
O	−1.91	−2.1	1037	O-O	22764	0.149031	20.37
Fe	3.82	2.5	121881	Fe-O	900	0.374532	0

a mode under a particular symmetry operation is obtained by $\chi = \mathbf{E_V} \cdot \mathbf{E_S}$, where $\mathbf{E_S}$ is the symmetry-transformed $\mathbf{E_V}$. We have repeated our calculations for CaMnO$_3$ with the parameters as in Ref. 19, and the results for symmetry assignments (shown in Fig. 3 of Ref. 19) agree exactly with ours, thus putting confidence in our calculations for the case of CFO. The eigenvector analysis of the optical modes of CFO gives 24 Raman-active modes. The frequencies of the five modes ($\mathbf{W_1} \cdots \mathbf{W_5}$) observed in our experiments are very close to the calculated Raman modes, thus helping us to assign the vibrational patterns of these modes, as given in Table I and shown in Fig. 2. The low-frequency $\mathbf{W_1}$(149 cm^{-1}) mode is associated with the A_g in-phase y rotation (seen at 160 cm^{-1} in CaMnO$_3$), the $\mathbf{W_2}$(197 cm^{-1}) mode is associated with the B_{1g} out-of-phase y rotation (seen at 179 cm^{-1} in CaMnO$_3$), and the $\mathbf{W_3}$(218 cm^{-1}) mode is associated with the A_g out-of-phase x rotation (seen at 184 cm^{-1} in CaMnO$_3$). The $\mathbf{W_4}$(305 cm^{-1}) mode is close to the calculated B_{1g} mode at 301 cm^{-1} associated with in-phase x rotation as well as to the B_{2g} (302 cm^{-1}) mode involving the mixed motion of Ca and O ions. It is also seen that LSFO has a Raman band at 307 cm^{-1}($\mathbf{M_2}$). Since the vibrational pattern of $\mathbf{W_4}$ and $\mathbf{M_2}$ modes is expected to be similar, they may not involve ions of very different masses (i.e., Ca vis-à-vis La and Sr).[22] Thus we associate the $\mathbf{W_4}$ mode with the B_{1g} in-phase x rotation of the adjacent FeO$_6$ octahedra, similar to the B_{1g} assignment of the $\sim$320 cm^{-1} mode in the rare-earth orthoferrites RFeO$_3$ (R=Y, Tb, Ho, Er, and Tm).[23] The $\mathbf{W_5}$(707 cm^{-1}) mode is associated with the B_{2g} symmetric stretching of the FeO$_6$ octahedra. The corresponding mode is seen at 611 cm^{-1} in LaMnO$_3$ (predicted by LDC to be at 669 cm^{-1}).[24] For isos-

tructural orthorhombic CaMnO$_3$, the LDC predicts the occurrence of this mode at 749 cm^{-1}. However, in CaMnO$_3$ this mode is experimentally not observed.[19] The reason for this has been attributed to the lack of JT distortion in CaMnO$_3$. Thus the presence of the $\mathbf{W_5}$ mode in the Raman spectra implies that some amount of JT-type distortion is present at room temperature in CFO, indicating the existence of a JT Fe^{4+} ionic state along with the non-JT, Fe^{3+}L, state. The LDC of CFO do not yield any phonon modes above 730 cm^{-1} and hence we expect the high-frequency modes $\mathbf{W_6}$(844 cm^{-1}), $\mathbf{W_7}$(898 cm^{-1}), and $\mathbf{W_8}$(922 cm^{-1}) to be due to the two-phonon Raman-scattering process, probably involving the $\mathbf{W_5}$ phonon along with other low-frequency modes. For example, the one-phonon density of states of CFO at room temperature[8] shows prominent bands at $\sim$137 cm^{-1} and $\sim$190 cm^{-1}. The $\mathbf{W_6}$ mode can be a combination of $\sim$707 cm^{-1} and $\sim$137 cm^{-1} phonons; $\mathbf{W_7}$ can be 707 cm^{-1} and 191 cm^{-1} and $\mathbf{W_8}$$\sim$707 cm^{-1} and 218 cm^{-1} modes.

The assignment of the Raman modes observed in LSFO was guided by the experimentally observed Raman modes and the LDC performed by Abrashev et al.[20] for the rhombohedral r-LaMnO$_3$. The $\mathbf{M_1}$(251 cm^{-1}) mode is assigned to the A_{1g} rotational mode of FeO$_6$ octahedra.[20] It corresponds to the observed mode at 236 cm^{-1} (249 cm^{-1} in LDC) in r-LaMnO$_3$. The other modes $\mathbf{M_2}$, $\mathbf{M_3}$, $\mathbf{M_4}$ are not close to any of the other four Raman-active modes calculated in r-LaMnO$_3$.[20] These four modes for r-LaMnO$_3$ are calculated to be at 42, 163, 468, and 646 cm^{-1}.[20] However, the frequencies of $\mathbf{M_2}$ and $\mathbf{M_3}$ are close to the calculated IR-active modes in r-LaMnO$_3$. Further, the temperature dependences of $\mathbf{M_2}$ and $\mathbf{M_3}$ are closely correlated with each other (to be discussed later). Hence we suggest that the $\mathbf{M_2}$ and $\mathbf{M_3}$ modes are IR-active A_{2u} and E_u bending modes of the FeO$_6$ octahedra.[20] These modes are calculated to be at 310 cm^{-1}[A_{2u}(TO)] and 357 cm^{-1}[E_u(TO)] in r-LaMnO$_3$.[20] Here TO stands for the transverse-optical mode. The corresponding longitudinal-optical (LO) modes calculated for r-LaMnO$_3$ are at 465 cm^{-1}[A_{2u}(LO)] and 488 cm^{-1}[E_u(LO)], whose signatures are not found in LSFO. The $\mathbf{M_4}$(704 cm^{-1}) feature is associated with the symmetry-forbidden symmetric-stretching mode of FeO$_6$, similar to the $\mathbf{W_5}$ mode seen in CFO. The $\mathbf{M_5}$(843 cm^{-1}), $\mathbf{M_6}$(897 cm^{-1}), and $\mathbf{M_7}$(920 cm^{-1}) modes occur almost at the same frequencies as $\mathbf{W_6}$, $\mathbf{W_7}$, and $\mathbf{W_8}$, respectively, and hence are assigned to two-phonon Raman scattering.

C. Temperature dependence of modes in CaFeO$_3$

Raman spectra of CFO at few selected temperatures are shown for various spectral ranges: (i) 100−350 cm^{-1} in Fig.

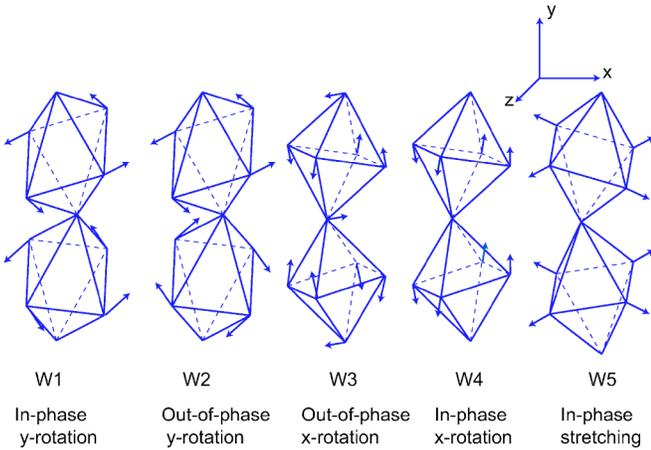| W1	W2	W3	W4	W5
In-phase y-rotation	Out-of-phase y-rotation	Out-of-phase x-rotation	In-phase x-rotation	In-phase stretching

FIG. 2. Vibrational pattern of the Raman active modes assigned to $\mathbf{W_1}$, $\mathbf{W_2}$, $\mathbf{W_3}$, $\mathbf{W_4}$, and $\mathbf{W_5}$ for CFO.

TABLE II. Comparison between the experiments and LDC calculation.

Assignment	Expt cm^{-1}	Calc. cm^{-1}	Vibrational Pattern
A_g	149 ($\mathbf{W}_1$)	171	In-phase y rotation
A_g	218 ($\mathbf{W}_3$)	209	Out-of-phase x rotation
A_g		280	Movement of Ca ions
A_g		316	Movement of Ca ions
A_g		347	Movement of Ca ions
A_g		522	Out-of-phase bending
A_g		540	In-phase stretching
B_{1g}	197 ($\mathbf{W}_2$)	190	Out-of-phase y rotation
B_{1g}	305 ($\mathbf{W}_4$)	301	In-phase x rotation
B_{1g}		375	Mixed motion of Ca and O ions
B_{1g}		537	Out-of-phase stretching
B_{1g}		670	Out-of-phase stretching
B_{2g}		168	Out-of-phase z rotation
B_{2g}		247	Motion of Ca
B_{2g}		302	Mixed motion of Ca and O ions
B_{2g}		385	Mixed motion of Ca and O ions
B_{2g}		519	Out-of-phase bending
B_{2g}		579	In-phase bending
B_{2g}	707 ($\mathbf{W}_5$)	708	In-phase stretching
B_{3g}		297	Motion of Ca
B_{3g}		340	In-phase z rotation
B_{3g}		518	Out-of-phase bending
B_{3g}		536	Out-of-phase stretching
B_{3g}		727	Out-of-phase stretching

3, (ii) 550–800 cm^{-1} in Fig. 4(a), and (iii) 750–1000 cm^{-1} in Fig. 5(a). It can be noted from Fig. 3 that the $\mathbf{W}_2$ mode is absent in the spectra below 175 K. The frequencies and the full width at half maximum (FWHM) of the modes $\mathbf{W}_1 \cdots \mathbf{W}_4$ show the usual temperature dependence: the frequencies increase by ~5 cm^{-1} and the FWHM decreases by ~5 cm^{-1} as temperature is lowered (not shown). The temperature behavior of the Raman band $\mathbf{W}_5$ (centered about 707 cm^{-1}) as shown in Fig. 4(a) is interesting. Above T_{co}, the mode appears at the same frequency in both the HH and HV polarizations. Below T_{co}, in HH polarization the asymmetric Raman line shape can be fitted to two modes: the main strong mode at ~707 cm^{-1} and a very weak mode at 684 cm^{-1}; in HV polarization, the structure is reversed. We suggest that the minor component is due to polarization leakage. In other words, below T_{co} the frequency of the main mode is ~707 cm^{-1} in HH polarization and ~684 cm^{-1} in HV polarization. The temperature dependence of the peak positions is shown in Fig. 4(b). Interestingly, above T_{co} the mode frequency increases with increasing temperature, which cannot be understood in terms of anharmonic interactions. The frequency of the mode in HH polarization increases slightly as the temperature is lowered. The activating distortion required for the observation of the symmetric-stretching mode in Raman scattering causes the deformation of the FeO$_6$ octahedra so that the square formed by the pla-
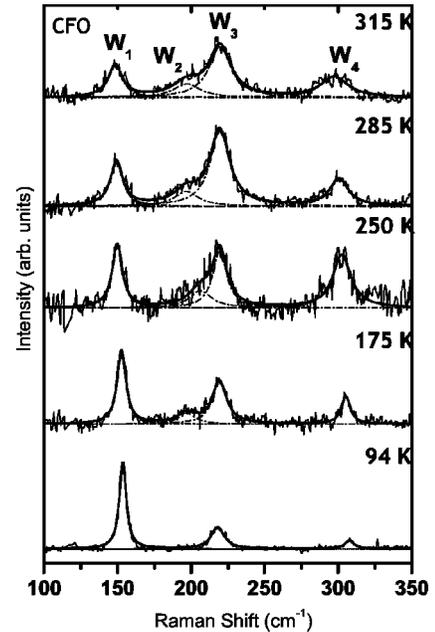

FIG. 3. Raman spectra of CFO for a few selected temperatures (shown by the side of the spectrum) in the spectral window 100–350 cm^{-1}. The dotted lines show Lorentzian fits to the data, which are resolved into four peaks, i.e., $\mathbf{W}_1$, $\mathbf{W}_2$, $\mathbf{W}_3$, and $\mathbf{W}_4$.
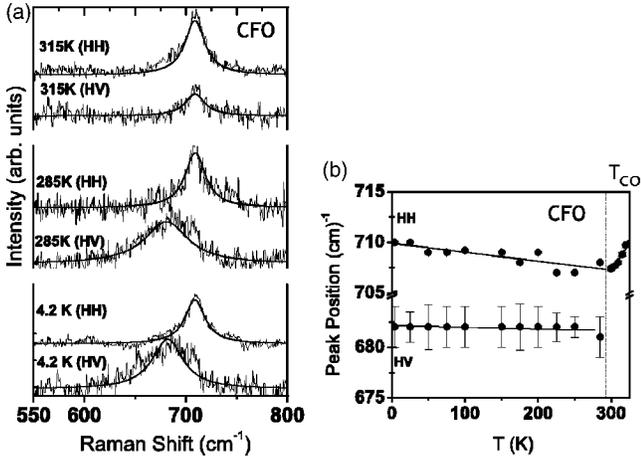
FIG. 4. (a) The HH and HV polarized spectra of the W_5 mode of CFO at a few temperatures. The solid lines are Lorentzian fits to the data. (b) The variation of W_5 mode as a function of temperature. The mode splits into a high-frequency (HH-polarized) and a low-frequency mode (HV-polarized) below T_{co} (290 K).

nar oxygen atoms transforms to a rhombus.[19] Below T_{co}, the charge disproportionation causes the arrangement of Fe^{3+} (large octahedra) and Fe^{5+} (small octahedra) in a rock-salt-type ordering of Fe^{3+} and Fe^{5+} ions such that each large octahedra is surrounded by six small octahedra in the low-temperature monoclinic ($P112_{1/a}$) phase of CFO.[3] This causes the distance between Fe and the two nonequivalent planar oxygens (O2,O3) to be different.[3] Fe^{5+}-O2=1.870 Å, Fe^{5+}-O3=1.894 Å, Fe^{3+}-O2=1.971 Å, and Fe^{3+}-O3=1.974 Å. This distortion would result in the observation of the symmetric-stretch mode below T_{co}. It has been experimentally observed that the stretching mode frequency has a ($d^{-1.5}$) dependence,[11] where d is the Fe-O distance. Thus the splitting of the 707 cm^{-1} in-phase stretching mode below T_{co}
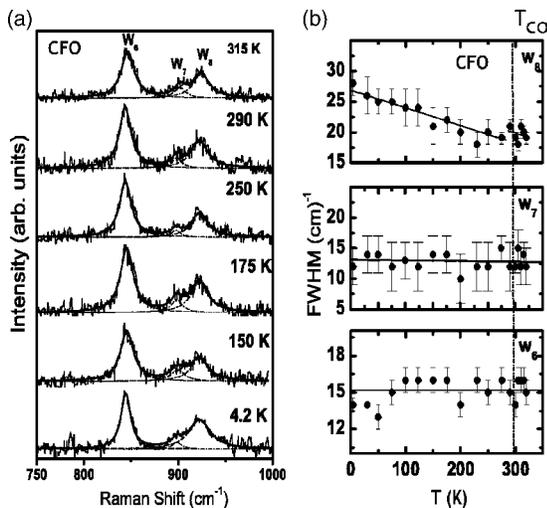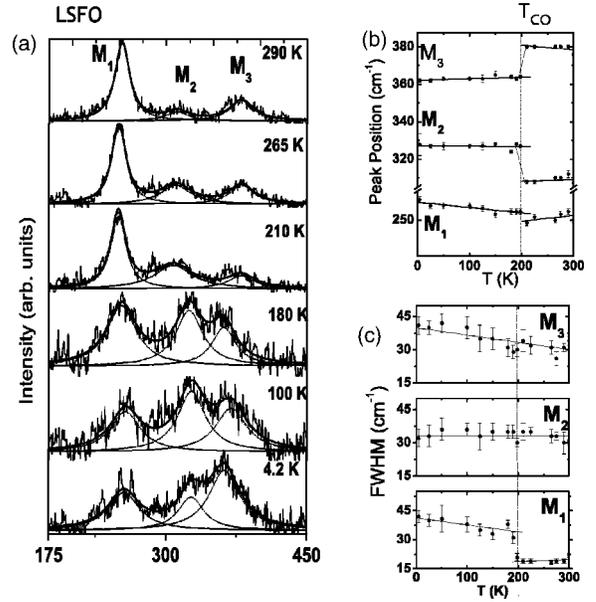

FIG. 6. Raman spectra of LSFO for a few selected temperatures (shown by the side of the spectrum) in the spectral window 175–450 cm^{-1}. The dotted lines show Lorentzian fits to the data, which were resolved into three peaks, i.e., M_1, M_2, and M_3. (b) Variation of peak positions and (c) FWHM with lowering of temperature.

can be attributed to the occurrence of two average Fe-O distances associated with the formation of the small and large octahedra in the charge-disproportioned state. The average Fe—O distance for the small octahedra is 1.872 Å and for the large octahedra 1.974 Å at 15 K in comparison to the 1.922 Å at room temperature.[3] Since $\Delta\omega/\omega = -1.5\Delta d/d$, the 707 cm^{-1} mode will split into two modes at 734 cm^{-1} and 680 cm^{-1}, which are close to the observed values seen in Fig. 4. However, the polarization dependence of the W_5 is not understood.

The peak positions of W_6, W_7, and W_8 remain almost constant with the lowering of temperature (not shown). Figures 5(a) and 5(b) show the temperature variation of the FWHM for these modes. The FWHM's of W_6 and W_7 do not change much with temperature. However, the temperature dependence of the FWHM of the W_8 mode is anomalous: it increases significantly below T_{co}. We do not have a quantitative understanding of this result. It is likely that below T_{co}, new modes can become Raman-active due to lowering of the crystal symmetry.[3] The increase in the FWHM can be due to inhomogeneous broadening arising from the appearance of new modes below T_{co}.

D. Temperature dependence of modes in LSFO

Raman spectra of LSFO at few selected temperatures are shown for various spectral ranges: (i) 175–450 cm^{-1} in Fig. 6(a) and (ii) 650–1000 cm^{-1} in Fig. 7(a). There are no spectral features between 450 and 650 cm^{-1}. The temperature dependence of the frequencies and the FWHM for the three modes M_1, M_2, and M_3 are shown in Figs. 6(b) and 6(c), respectively. It can be seen that for the M_1 mode, the peak

FIG. 5. Raman spectra of CFO for a few selected temperatures (shown by the side of the spectrum) in the spectral window 650–1000 cm^{-1}. The dotted lines show Lorentzian fits to the data, which were resolved into three peaks, i.e., W_6, W_7, and W_8. (b) The variation of the FWHMs with lowering of temperature.
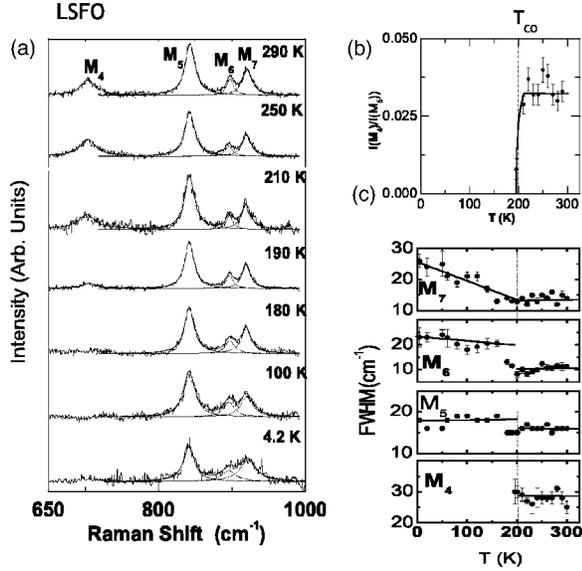
FIG. 7. Raman spectra of LSFO for a few selected temperatures (shown by the side of the spectrum) in the spectral window 650–1000 cm^{-1}. The dotted lines show Lorentzian fits to the data, which were resolved into four peaks, i.e., M_4, M_5, M_6, and M_7. (b) Intensity of the M_4 peak normalized to that of the M_5 with lowering of temperature and (c) variation of FWHMs with lowering of temperature.

position and the FWHM show sharp changes at T_{co} of 200 K. Most interestingly, the FWHM of the M_1 mode increases as temperature is lowered. The peak positions of M_2 and M_3 modes also show a discontinuous change at T_{co} in opposite directions, i.e., the peak position of M_2 increases while that of M_3 decreases with temperature. As discussed earlier, we have attributed M_2 and M_3 to the disorder-activated A_{2u} and E_u bending modes, respectively. It has been shown[20] that the A_{2u}-E_u separation for a given pair is a direct measure of the rhombohedral distortion in the structure, i.e., when the rhombohedral distortions are small, the A_{2u}-E_u separation is also small compared to, e.g., LO-TO splitting. The temperature dependence of M_2 and M_3 mode frequencies seen in Fig. 6(b) will imply that the rhombohedral distortion has reduced abruptly at T_{co}. This inference of the reduction of the rhombohedral distortions below T_{co} in LSFO from the Raman data is in contrast to the neutron-scattering results, which predict a small increase in the rhombohedral distortions,[6,7] i.e., an increase in the Fe-O-Fe bond angle as well as rotational distortions. The angle α, a measure of the rotational distortion, is related to the x parameter of the oxygen $6e$ site position in $R\bar{3}c$ structure and is given by $x = 1/2(1 \pm 1/\sqrt{3}\tan^{-1} \alpha)$. Using the values of x for LSFO,[6] $\alpha = 3.8°$ at room temperature and $\alpha = 5.2°$ at 50 K. However, it needs to be kept in mind that the changes in the value of the Fe-O-Fe bond angle and the x parameter of the oxygen $6e$ site obtained from the neutron-scattering data were derived by assuming an $R\bar{3}c$ structure for the low-temperature phase as well. This assumption need not be correct, and has been pointed out by Yang et al.[7]

From Fig. 7(a), we note that the intensity of the M_4 mode with respect to the intensity of the M_5 mode is different from that shown in Fig. 1(b). This is because the sample is polycrystalline and hence grains with different orientations are being recorded in experiments outside the cryostat [Fig. 1(b)] and in the cryostat [Fig. 7(a)]. It can be further seen from Fig. 7(a) that the intensity of the M_4 mode at 707 cm^{-1} decreases as temperature is lowered and is not observed below T_{co}. The variation of the intensity of the M_4 mode normalized to the intensity of the M_5 mode is given in Fig. 7(b). Recall that the M_4 mode associated with the symmetric-stretching mode is forbidden in the $R\bar{3}c$ structure. Above T_{co} it becomes Raman-active, perhaps due to local distortions of the FeO$_6$ octahedra. Below T_{co}, the absence of the M_4 mode implies that such distortions of the octahedra are not present in LSFO.[6,7] This is consistent with the lowering of the rhombohedral distortion inferred from the temperature dependence of the M_2 and M_3 mode frequencies. The peak positions of the $M_4\cdots M_7$ modes do not change significantly with temperature (data not shown). The temperature variation of the FWHM of these modes is shown in Fig. 7(c). The FWHM's of M_5, M_6, and M_6 increase as temperature is lowered, showing a distinct discontinuity at T_{co}. This is similar to the temperature dependence of the W_8 mode [see Fig. 5(b)] and hence the increase in the FWHM's could possibly be due to inhomogeneous broadening due to the appearance of new modes below T_{co}.

E. Discussion and summary

We have studied the temperature dependence of Raman spectra of CFO and LSFO across charge ordering and magnetic transitions. The spectra show one-phonon Raman scattering in the spectral range 100–750 cm^{-1} and two-phonon Raman scattering between 800 and 1000 cm^{-1}. An interesting point to note is that the intensity of the two-phonon bands is comparable to the first-order Raman bands. Such strong second-order Raman scattering has been predicted for manganites involving vibrationally excited self-trapped orbitons from the orbitally ordered Jahn-Teller ground state.[25] Recalling that below T_{co} the disappearance of the symmetric-stretching mode (M_4) for LSFO suggests a reduction of JT distortions, it is unlikely that this mechanism is responsible for observation of the strong two-phonon bands.

The observation of the bond-stretching mode in Raman spectra indicates that there is a JT distortion of the FeO$_6$ octahedra due to the mixture of the Fe^{4+}(d^4)-like configuration into the predominant d$^5\underline{L}$ configuration. Because the Raman spectra of both CFO and LSFO show a symmetric-stretching mode above T_{co}, their electronic structures are similar in that temperature range. Below T_{co}, the stretching mode is seen only for CFO, meaning that the distortion persists only in CFO. A possible reason for this can be that the charge disproportionation is incomplete in CFO because it is enforced by the lattice distortion, whereas in LSFO, the charge disproportionation is rather complete because the electronic system spontaneously charge disproportionates. The splitting of the symmetric-stretching (W_5) mode below the transition temperature (290 K) is seen due to the presence of small and large octahedra (arising from Fe^{5+} and Fe^{3+} states, respectively). In LSFO, the symmetric-stretching

mode $\mathbf{M}_4$, though not Raman-active in the $R\bar{3}c$, is seen above T_{co}. This would imply that the distance between the two pair of planar oxygen atoms is not equal, i.e., JT-type distortions are present in LSFO. The disappearance of this mode below T_{co} implies the absence of this distortion in the low-temperature phase. This is also corroborated by the temperature dependence of the $\mathbf{M}_2$ and $\mathbf{M}_3$ modes, which have been assigned to the disorder-activated A_u and E_u IR modes. The difference in $\mathbf{M}_2$ and $\mathbf{M}_3$ mode frequencies, which is related to the rhombohedral distortion of the adjacent FeO_6 octahedra, decreases abruptly at T_{co}.

Let us compare our Raman results to the changes in the phonon density of state (DOS) measured by the nuclear resonant x-ray inelastic scattering.[8] The changes in the DOS between the spectral range of $300-500$ cm^{-1} across T_{co} in CFO were much more pronounced than that in LSFO. This is the region encompassing the $\mathbf{W}_4$ mode in CFO and the $\mathbf{M}_2$ and $\mathbf{M}_3$ modes in LSFO. The mode frequencies of $\mathbf{M}_2$ and $\mathbf{M}_3$ show significant changes across T_{co}. The large change seen in Raman scattering vis-à-vis small changes in DOS seen by the nuclear resonant x-ray inelastic scattering can be understood from the fact that the DOS at a given frequency is a sum over all the phonon states in the Brillouin zone while first-order Raman scattering investigates the behavior of a mode at the center of the Brillouin zone. On the other hand, in the case of CFO, more pronounced changes are seen in the DOS (Ref. 8) between 300 and 500 cm^{-1} across T_{co} than for the $\mathbf{W}_4$ mode (the only observed Raman mode in that spectral range). This implies that in CFO, in the spectral range from 300 to 500 cm^{-1}, the phonons other than the zone-center Raman-active ones are affected across T_{co}.

To sum up, more theoretical understanding has yet to emerge to explain quantitatively the observation of the strong second-order Raman scattering in these systems, the polarization dependence of the symmetric stretching mode ($\mathbf{W}_5$) in CFO, and the temperature dependence of the $\mathbf{M}_2$ and $\mathbf{M}_3$ modes in LSFO. We hope that our present detailed Raman study will motivate this.

*Corresponding author. Email address: asood@physics.lisc.ernet.in

[1] M. Imada, A. Fujimori, and Y. Tokura, Rev. Mod. Phys. **70**, 1039 (1998).

[2] M. Abbate, G. Zampieri, J. Okamoto, A. Fujimori, S. Kawasaki, and M. Takano, Phys. Rev. B **65**, 165120 (2002).

[3] P. M. Woodward, D. E. Cox, E. Moshopoulou, A. W. Sleight, and S. Morimoto, Phys. Rev. B **62**, 844 (2000).

[4] J. Matsuno, T. Mizokawa, A. Fujimori, Y. Takeda, S. Kawasaki, and M. Takano, Phys. Rev. B **66**, 193103 (2002).

[5] J. Q. Li, Y. Matsui, S. K. Park, and Y. Tokura, Phys. Rev. Lett. **79**, 297 (1997).

[6] P. D. Battle, T. C. Gibb, and P. Lightfoot, J. Solid State Chem. **84**, 271 (1990).

[7] J. B. Yang *et al.*, J. Phys.: Condens. Matter **15**, 5093 (2003).

[8] J. Matsuno, M. Seto, S. Kitao, Y. Kobayashi, Y. T. S. K. R. Haruki T. Mitsui, A. Fujimori, and M. Takano, J. Phys. Soc. Jpn. **73**, 2768 (2004).

[9] R. Gupta, A. K. Sood, P. Metcalf, and J. M. Honig, Phys. Rev. B **65**, 104430 (2002).

[10] R. Gupta, G. V. Pai, A. K. Sood, T. V. Ramakrishnan, and C. N. R. Rao, Europhys. Lett. **58**, 778 (2002).

[11] L. Martín-Carron, A. deAndrés, M. J. Martínez-Lope, M. T. Casais, and J. A. Alonso, Phys. Rev. B **66**, 174303 (2002).

[12] M. N. Iliev, and M. V. Abrashev, J. Raman Spectrosc. **32**, 805 (2001).

[13] S. Yoon, M. Rübhausen, S. L. Cooper, K. H. Kim, and S. W. Cheong, Phys. Rev. Lett. **85**, 3297 (2000).

[14] E. Granado, N. O. Moreno, A. García, J. A. Sanjurjo, C. Rettori, I. Torriani, S. B. Oseroff, J. J. Neumeier, K. J. McClellan, S. W. Cheong, and Y. Tokura, Phys. Rev. B **58**, 11 435 (1998).

[15] S. Kawasaki, M. Takano, R. Kanno, T. Takeda, and A. Fujimori, J. Phys. Soc. Jpn. **67**, 1529 (1998).

[16] M. Takano, J. Kawachi, N. Nakanishi, and Y. Takeda, J. Solid State Chem. **39**, 75 (1981).

[17] M. Takano, S. Nasu, T. Abe, K. Yamamoto, S. Endo, Y. Takeda, and J. B. Goodenough, Phys. Rev. Lett. **67**, 3267 (1991).

[18] Sung Hyun Yoon and Chul Sung Kim, J. Korean Phys. Soc. **44**, 369 (2004).

[19] M. V. Abrashev, J. Backstrom, L. Borjesson, V. N. Popov, R. A. Chakalov, N. Kolev, R. L. Meng, and M. N. Iliev, Phys. Rev. B **65**, 184301 (2002).

[20] M. V. Abrashev, A. P. Litvinchuk, M. N. Iliev, R. L. Meng, V. N. Popov, V. G. Ivanov, R. A. Chakalov, and C. Thomsen, Phys. Rev. B **59**, 4146 (1999).

[21] A. Mirone, OpenPhononSourceCode, http://www.˜esrf.˜fr.˜/ computing/scientific.

[22] The frequency of a mode involving the motion of an element Ca, La/Sr is expected to scale inversely as the square root of the mass of the element. Since the mass of the La/Sr ion is much larger than the Ca ion, one would expect that a similar mode involving the motion of La/Sr in the case of LSFO would be shifted to lower frequency as compared to the mode involving the motion of Ca ions in CFO, but this is not the case here.

[23] S. Venugopalan, M. Dutta, A. K. Ramdas, and J. P. Remeika, Phys. Rev. B **31**, 1490 (1985).

[24] M. N. Iliev, M. V. Abrashev, H. G. Lee, V. N. Popov, Y. Y. Sun, C. Thomsen, R. L. Meng, and C. W. Chu, Phys. Rev. B **57**, 2872 (1998).

[25] P. B. Allen and V. Perebeinos, Phys. Rev. Lett. **83**, 4828 (1999).